PAPER

Check for updates

Investigation of structural, optical and electrical conductivity of a new organic inorganic bromide: [C₁₂H₁₇N₂]₂ZnBr₄†

I. Kammoun, ID *a M. Belhouchet, ID b A. Ben Ahmed, ID c J. Lhoste ID d and M. Gargouria

A new organic–inorganic hybrid, namely the [C₁₂H₁₇N₂]₂ZnBr₄ compound, has been synthesized and studied by single-crystal X-ray diffraction and optical and complex impedance spectroscopy. It crystallized in the centrosymmetric $P2_1/n$ space group at room temperature. The asymmetric unit is constituted by $[ZnBr_4]^{2-}$ anions, showing slightly distorted tetrahedral geometry, surrounded by four organic $(C_{12}H_{17}N_2)^+$ cations. The crystal packing is stabilized by N–H⋯Br and C–H⋯Br hydrogen bonds arranged in a three-dimensional network. The optical absorption measurement confirms the semiconductor nature with a band gap of around 3.94 eV. Additionally, the analysis of Nyquist plots ($-Z''$ vs. Z') shows that the electrical properties of the material are heavily dependent on frequency and temperature, indicating a relaxation phenomenon and semiconductor-type behavior. Reduction in Z' was observed as a function of temperature and frequency which indicates an increase in ac conductivity and the negative temperature coefficient of resistance. The frequency dependent plots of ($-Z''$) show that the electrical relaxation is non-Debye in nature. The ac conductivity spectrum obeys Jonscher's universal power law. The Correlated barrier hopping model CBH has been suggested to agree with the conduction mechanism of σ_{ac} for the [C₁₂H₁₇N₂]₂ZnBr₄ compound.

1. Introduction

In recent years, organic–inorganic hybrid compounds have constituted a large class of materials thanks to the improvement of their physico-chemical properties through which it was possible to gather both organic and inorganic components as well as outstanding properties from the different parts.[1–3] A special place in this group of materials is occupied by organic–inorganic hybrids based on divalent metal halides (Cu, Zn, Co, Ni…) whose temperature-dependent optical and electrical properties are relevant for emerging applications in optical devices, information storage, solar cells, photocatalysts, etc.[4–8] An important feature of organic–inorganic hybrids is their structural tenability. In fact, some structural differences are observed if the counter ions of the inorganic parts are monoprotonated or diprotonated amines. The crystallographic orientation and the thickness of the inorganic sheets may vary according to the choice of the appropriate organic cations.[9,10] Due to the structural flexibility of the hybrid compound, the choice of different organo-ammoniums to stabilize various orientations or dimensions of inorganic sheets is an interesting area to explore the relationship between structures and physico-chemical properties within a single structure family.[11,12] The organic divalent zinc bromide has several applications in various domains such as catalysis, biochemistry, dielectric transition and magnetism material science. In addition, the study of such zinc-based materials has received much attention recently in the light of photovoltaic and multifunctional properties.[13]

The new [C₁₂H₁₇N₂]₂ZnBr₄ compound has therefore been prepared with the aim of studying its optical and electrical properties by using UV-vis and complex impedance spectroscopy, respectively. Its crystal structure was determined from X-ray diffraction data collected on a single crystal obtained by the slow evaporation method.

2. Experimental

2.1. Synthesis

The synthesis of the [C₁₂H₁₇N₂]₂ZnBr₄ sample was carried out using the reported preparation procedure.[14] The organic parts

aUniversity of Sfax, Faculty of Sciences, Laboratory of Spectroscopic Characterization and Optical Materials, 3018 Sfax, BP1171, Tunisia. E-mail: kammoun.fss@gmail.com
bPhysico-Chemistry of Solid State Laboratory, Department of Chemistry, Faculty of Sciences of Sfax, 3000 Sfax, BP1171, Tunisia
cUniversity of Sfax, Faculty of Sciences of Sfax, Department of Physic, Laboratory of Applied Physic, B.P. No. 802, 3018 Sfax, Tunisia
dInstitute for Molecules and Materials Le Mans, University of Maine, Avenue Olivier Messiaen, 72085 Le Mans Cedex 9, France

1,2-phenylenediamine (purity 99.5%, FLUKA) was dissolved in acetone and $ZnBr_2$ (purity 98%, FLUKA), dissolved in hydrochloric acid solution (1 M), in molar ratio 2 : 1. By slow evaporation at room temperature, yellow crystals suitable for X-ray single crystal analysis were obtained.

2.2. X-ray data collection

Single crystal sized (0.35, 0.25, 0.20) mm^3 was carefully selected to perform its structural analysis by X-ray diffraction. The crystallographic data were collected on a Bruker AXS CCD diffractometer at room temperature using graphite-monochromated Mo Kα radiation ($\lambda = 0.71073$ Å). All intensities were corrected for Lorentz, polarization and absorption effects.[15] The structural determination procedure was carried out using SHELXS97 program.[16] The structure was solved by direct method and refined with full-matrix least squares methods based on F^2 using SHELXL97.[17] The space group was determined to be $P2_1/n$. A total of 54568 reflections were collected in the θ range 2.2–27.5°. In this structure, all non-hydrogen atoms were refined with anisotropic displacement parameters. H-atoms were set in calculated positions and treated as riding on their parent atom with constrained thermal parameters. The final discrepancy factors R_1 and wR_2 are 0.053 and 0.134, respectively. Crystal data of $(C_{12}H_{17}N_2)_2ZnBr_4$ are given in Table 1. Molecular plots were made with ORTEP[18] and Diamond.[19]

Atomic coordinates anisotropic displacement parameters, tables for all bond distances, and angles have been deposited at the Cambridge Crystallographic Data Centre (deposition number: CCDC 2090035).

2.3. Impedance spectroscopy

Furthermore, the impedance measurements of the investigated $[C_{12}H_{17}N_2]_2ZnBr_4$ compound were performed using two platinum electrodes. As a fact, the fine grain samples were pressed into a cylindrical pellet of typical dimension 8 mm diameter and 1.1 mm thickness pressed at a pressure of 3 ton per cm^2. Then, thin gold films, (with a thickness of a few nanometers), were manually deposited on both flat faces of the pellet. The measurements were performed as a function of both temperature and frequency employing using an 1260 Solartron Impedance Analyzer.

2.4. UV-visible measurements

UV-visible measurement was carried out using a conventional UV-visible spectrophotometer (HITACHI, U-3300) in the range 200–800 nm.

3. Results and discussion

3.1. Crystal structure

As shown in Fig. 1, the asymmetric unit is constituted by one tetabromozincate $[ZnBr_4]^{2-}$ anion and two protonated $[C_{12}H_{17}N_2]^+$ cations. The zinc atom is coordinated to four Br atoms forming a slightly distorted tetrahedron, as it can be deduced from the value of both the Zn–Br bond lengths, ranging from 2.3638(11) to 2.4464(10) Å, and the Br–Zn–Br angles, ranging from 105.35(4)° to 113.89(4)° (Table S1)†. The structural parameters of the present compound agree well with those found in similar compounds characterized by $[ZnBr_4]^{2-}$ tetrahedral units.[20]

The two chemically identical monoprotonated cations $[C_{12}H_{17}N_2]^+$ are crystallographically independent and are noted respectively: Cation (A) {N1a, N2a} and Cation (B) {N2a, N2b}. The values of C–C and C–N distance, in the two cations, range from 1.284(8) to 1.539(10) Å while C–C–C and C–C–N angles are between 105.2(7) and 133.3(6) (Table S2)†. Both cations are ordered and have slightly different torsions angles.[21,22]

The atomic arrangement of the studied compound is built of alternated organic and inorganic layers (Fig. 2). The crystal packing is stabilized by cation-to-anion N–H⋯Br and C–H⋯Br hydrogen bonds (four simple and one bifurcated) leading to a three-dimensional network. Hydrogen bonding parameters are listed in Table S3.† In this structure each $[ZnBr_4]^{2-}$ anions is surrounded by four organic $(C_{12}H_{17}N_2)^+$ cations (one cation A and three cations B (Fig. 3),). In addition, no face-to-face π–π interactions exist since the distance between centroid phenyl rings is equal to 7 Å.

3.2. Electrical impedance spectroscopy

Impedance spectroscopy is the most important technique to study the dynamics of mobile and bound charges in the bulk and interfacial areas of the materials. Generally, help in identifying the grain, grain boundary and electrode interface contributions in the polarization mechanism.[23,24]

Fig. 4 shows the variation of real part of the impedance (Z') with frequency at different temperatures. At low frequencies, the magnitude of Z' increases with the temperature at range from 353 K to 373 K. Then it is observed that beyond 373 K, the value of Z' decreases on increasing temperature, which can be

Table 1 Crystal data and structure refinement of $[C_{12}H_{17}N_2]_2[ZnBr_4]$

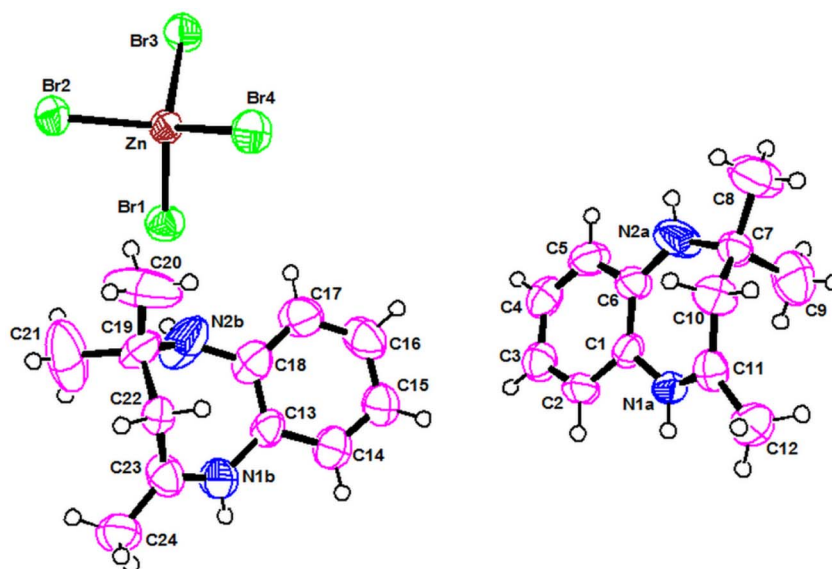|	
Empirical formula	$[C_{12}H_{17}N_2]_2[ZnBr_4]$
Formula weight	763.56
Temperature (K)	296
Wavelength (Å)	0.71073
Crystal system, space group	Monoclinic, $P2_1/n$
Unit cell dimensions	
a (Å)	12.1363(6)
b (Å)	14.9001(8)
c (Å)	16.2525(9)
β (°)	98.612(2)
V (Å^3)	2905.8(3)
Z	4
Density (calculated) (g cm^{-3})	1.745
Reflections collected	54568
Independent reflections	6663
Reflections observed with $I > 2\sigma(I)$	3046
R_{int}	0.136
Number of refined parameters	298
Goodness-of-fit on F^2	0.99
Final R indices [$I > 2\sigma(I)$]	$R_1 = 0.053$ and w$R_2 = 0.134$
Largest diff. peak and hole, e Å^{-3}	1.02 and −0.90
CCDC no.	2 090 035

Fig. 1 Molecular structure of the asymmetric unit of $[C_{12}H_{17}N_2]_2[ZnBr_4]$.

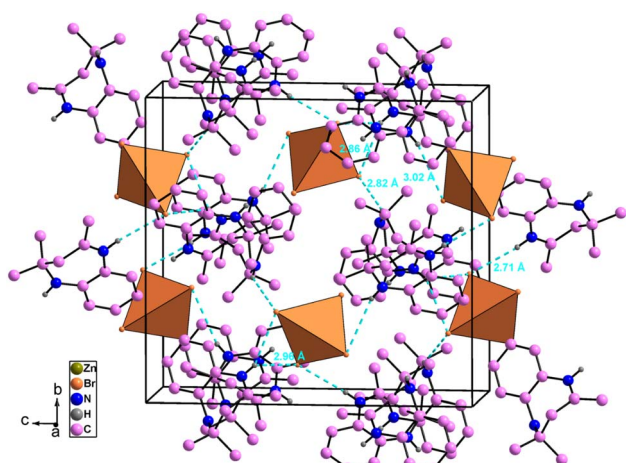**Fig. 2** Crystal packing of $[C_{12}H_{17}N_2]_2[ZnBr_4]$ compound in the (b, c) plane (hydrogen bonds shown as dashed lines).

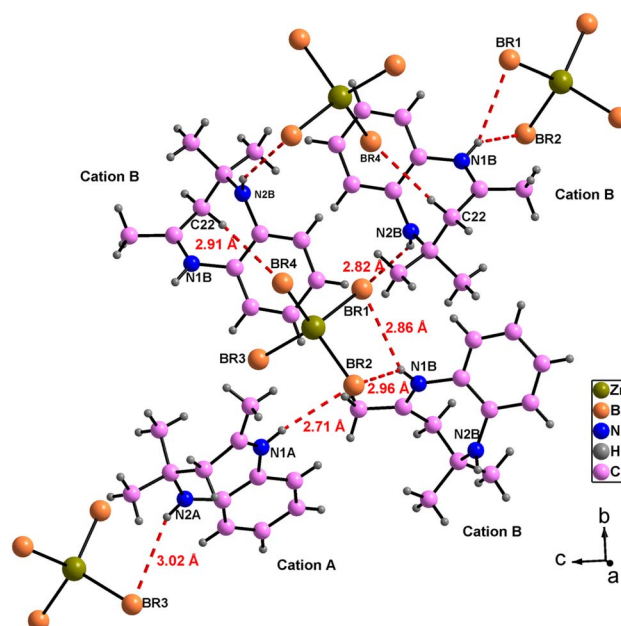**Fig. 3** Hydrogen bonding around $[ZnBr_4]^{2-}$ anions.

explained by the reduction of trapped charge density and a thermal activation of their mobility.[25] Besides, the values of Z' merge at high frequencies (>10^4 Hz). This can be understood by the fact that charge carriers acquired sufficient energy to overcome the potential barrier.[26]

Fig. 5 shows the temperature-dependent variations of the imaginary part ($-Z''$) as a function of frequency over the temperature range of 353 K to 443 K. The peaks appearing in the plots of frequency *versus* Z''_{max} were found to shift towards the side of higher frequencies. Furthermore, the broadening of peaks and decreasing value of Z''_{max} with increasing temperature, indicating the fact that multiple relaxation processes are occurring simultaneously.[27]

The Nyquist plot between the real Z' and imaginary ($-Z''$) part of impedance is used to analyze the conduction mechanism in any sample. These graphs usually appear in the form of

semicircles and each semicircle is a manifestation of unique relaxation process.[28]

Fig. 6 shows the imaginary part of the impedance ($-Z''$) *versus* the real part (Z') over a wide range of frequencies and at different temperatures. The colored symbols demonstrate the actual experimental data, whereas the solid-red lines represent the fit administered by Zview software.[29] This spectrum is characterized by the appearance of semicircular arc centered below the real axis which is temperature dependent. Depression of semicircle is originated from the presence of distribution of relaxation times. The radius of semicircle decreases with
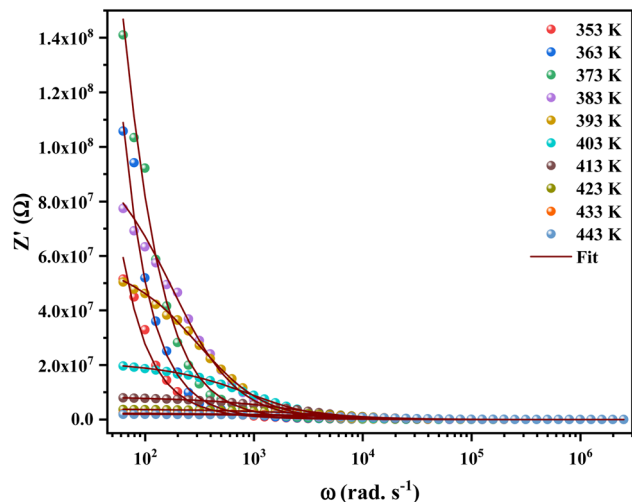
Fig. 4 Variation of the real part (Z') of the impedance of $[C_{12}H_{17}N_2]_2ZnBr_4$ compound as a function of angular frequency for different temperatures.
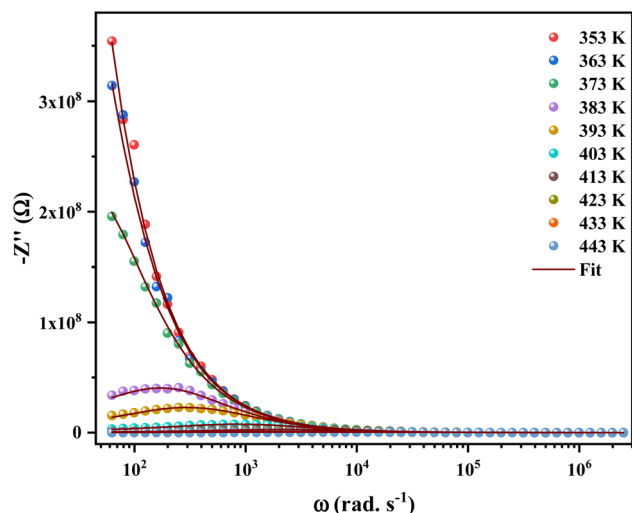

Fig. 5 Variation of imaginary part (Z'') with angular frequency in the measured temperature range.

increasing temperature due to increase in conductivity of the material. In reality, the non-Debye type of relaxation is obtained which obeys Cole–Cole model.[30] In order to analyze these spectra and to extract the different electrical parameters, an equivalent circuit model was proposed from the fit of experimental data to investigate the relationship between microstructure and electrical properties of sample. The best fit using Zview software was obtained using an equivalent circuit formed by a parallel combination of bulk resistance R capacitance C, and fractal capacitance CPE as depicted in the inset of Fig. 6. The constant phase element (CPE) is evaluated from the formula:

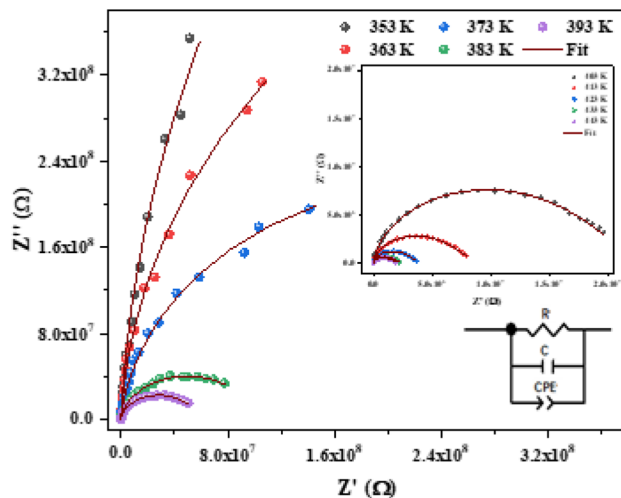$$Z_{CPE} = \frac{1}{Q(j\omega)^{\alpha}} \quad (1)$$

Fig. 6 Nyquist plot fitted with an equivalent circuit for $[C_{12}H_{17}N_2]_2$-$ZnBr_4$ compound at different temperatures.

where, Q is the capacitance value of the CPE impedance and ($0 < \alpha < 1$) relates to the deviation degree with respect to the pure capacitor value.

The theoretical values of the real (Z') and imaginary ($-Z''$) parts of the complex impedance, derived from the equivalent circuit, were deduced using the following expressions:

$$Z' = \frac{R^{-1} + Q\omega^{\alpha}\cos\left(\frac{\alpha\pi}{2}\right)}{\left(R^{-1} + Q\omega^{\alpha}\cos\left(\frac{\alpha\pi}{2}\right)\right)^2 + \left(C\omega + Q\omega^{\alpha}\sin\left(\frac{\alpha\pi}{2}\right)\right)^2} \quad (2)$$

$$-Z'' = \frac{C\omega + Q\omega^{\alpha}\sin\left(\frac{\alpha\pi}{2}\right)}{\left(R^{-1} + Q\omega^{\alpha}\cos\left(\frac{\alpha\pi}{2}\right)\right)^2 + \left(C\omega + Q\omega^{\alpha}\sin\left(\frac{\alpha\pi}{2}\right)\right)^2} \quad (3)$$

The parameters R, C, α and CPE obtained from the fitting results were evaluated and listed in Table 2. An overview in this table, the bulk resistance R decreases with increasing temperature, this behavior is related to increasing the mobility of charge carriers.[31]

The justification of the choice of the equivalent circuit is confirmed by the variations of the experimental values of (Z')

Table 2 The extract parameters for the circuit elements

T (K)	R (Ω)	C (10^{-11} F)	Q (10^{-11} F)	α
353	2.83×10^9	1.56	3.34	0.960
363	1.19×10^9	2.09	3.07	0.943
373	5.06×10^8	3.27	4.93	0.785
383	1.06×10^8	3.46	20	0.621
393	6.18×10^7	3.47	30.7	0.588
403	2.23×10^7	3.49	84	0.513
413	8.76×10^6	3.50	205	0.461
423	4.04×10^6	3.50	434	0.426
433	2.45×10^6	3.47	755	0.414
443	2.15×10^6	3.44	960	0.412

and $(-Z'')$ at various temperatures *versus* the calculated ones using the parameters of the equivalent circuit model (Fig. 7a and b). From this figure, it is evident that the slope obtained from a linear fit of the data points at each temperature is nearly equal to the unity. This behavior reveals that the adopted equivalent circuit describes well the electric properties of the investigated compound.

The electrical conductivity can be a well-established process for describing the hopping dynamics of the frees carriers. The obtained values of bulk resistance (R), corresponding to the grain, are used to determine the electrical conductivity sg as follows:

$$\sigma_g = \frac{e}{S \times R_g} \quad (4)$$

where e is sample thickness, S is the area of the pallet, R_g is grain resistance.

Fig. 8 shows the variation of the conductivity σ_g for grains. The linearity of $\ln(\sigma_g)$ *versus* $1000/T$ justifies that the title compound does not have a phase transition in the temperature range studied. We note that the conductivity increases with
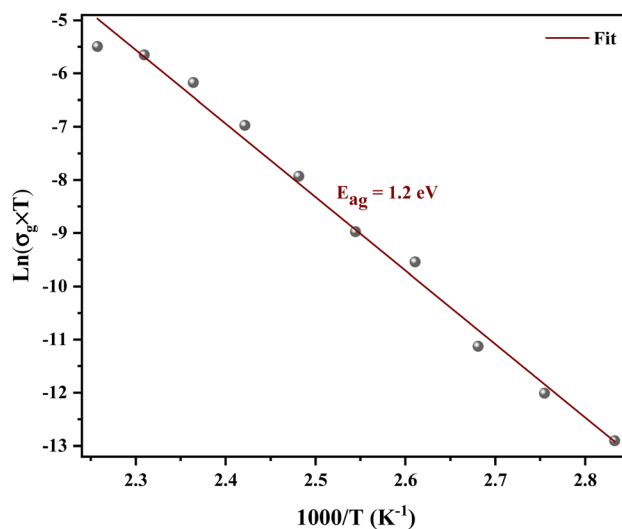
Fig. 8 Arrhenius plots for the bulk conductivity of the $[C_{12}H_{17}N_2]_2$-$ZnBr_4$ sample.

increase in temperature, which indicates the semiconductor behavior.[32] The linear region is fitted with the Arrhenius equation:

$$\sigma_g = \sigma_0 \exp\left(-\frac{E_a(\sigma)}{k_B T}\right) \quad (5)$$

where σ_g is electrical conductivity, σ_0 is the pre-exponential factor, k_B is the Boltzmann constant and E_a is the activation energy. The value of activation energy E_a can be determined from the linear fit is equal to: $E_a = 1.2$ eV. This activation energy E_a is similar to the values obtained previously.[32–34]

3.3. *ac* conductivity analysis

ac conductivity analysis helps to identify the type of transport for the charge carriers, which is responsible for the conduction process and its response as a function of frequency and temperature.[35]

The angular frequency dependence of the *ac* conductivity at several temperatures for $[C_{12}H_{17}N_2]_2ZnBr_4$ compound is shown in Fig. 9. The conductivity spectrum can be visually defined for two distinct regions. In the first region, a plateau is remarked at a low frequency up to a specific value known as the hopping frequency $\omega_h = 10^5$ rad s^{-1}, which indicates a frequency-independent conductivity. The conductivity increasing with temperature, this implies a semiconductor behavior for the prepared sample.[36] For the second region, the conductivity increases with increasing frequency. Moreover, to identify the suitable mechanism *ac* conductivity, an analysis of the frequency and conductivity (σ_{ac}) data are fitted by the Jonscher power law:[37]

$$\sigma_{ac}(\omega) = \sigma_{dc} + A\omega^s \quad (6)$$

where σ_{dc} is the *dc* conductivity, s represents the degree of interaction between mobile ions and the environments
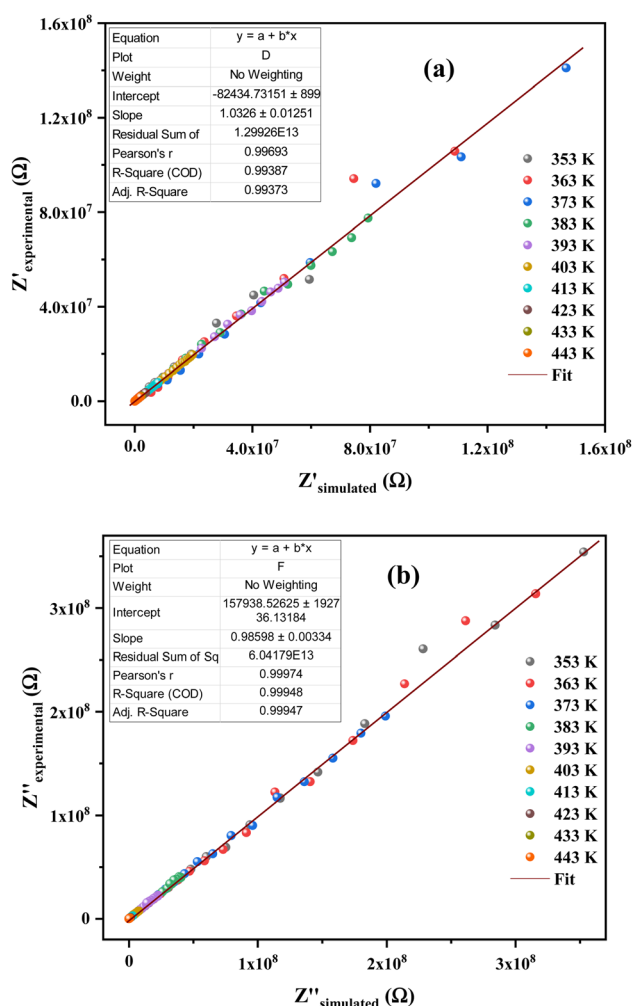
Fig. 7 (a) and (b) Plots of measured values *versus* simulated values of the real and imaginary parts of the impedance.
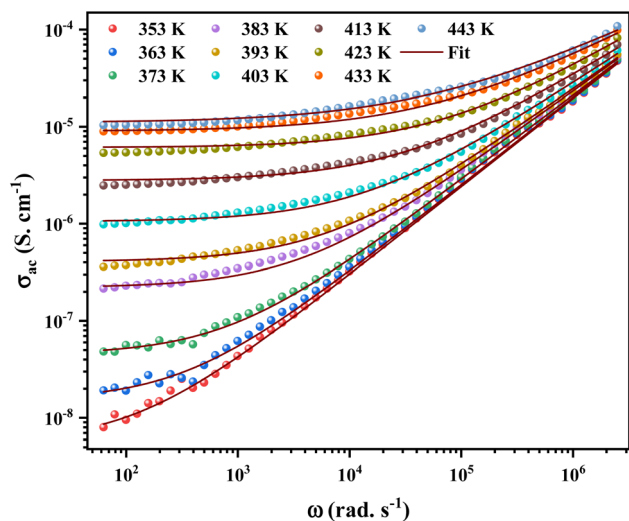
Fig. 9 Variation of the total conductivity as a function of angular frequency at different temperatures for $[C_{12}H_{17}N_2]_2ZnBr_4$ compound. Red solid lines represent the fitting to the experimental data using the universal Jonscher power law.

surrounding them and A is a constant. The A and s factors vary according to the temperature and the nature of the sample.

To define the predominant conduction mechanism of the ac conductivity of $[C_{12}H_{17}N_2]_2ZnBr_4$ compound, several theoretical models correlating the conduction mechanism with the exponent $s(T)$ behavior were used to determine this objective. We have fitted the ac conductivity data by using eqn (4) and the best fits can be obtained by consecutively varying A and s parameter.

From Fig. 10 it is possible to determine the conduction process in the prepared sample. Thus, s tends to decrease with increasing temperature. This decreasing trend behavior of s with temperature suggests that the conduction mechanism in the compound can be explained by the Correlated Barrier Hopping (CBH) model in the sample.[38]
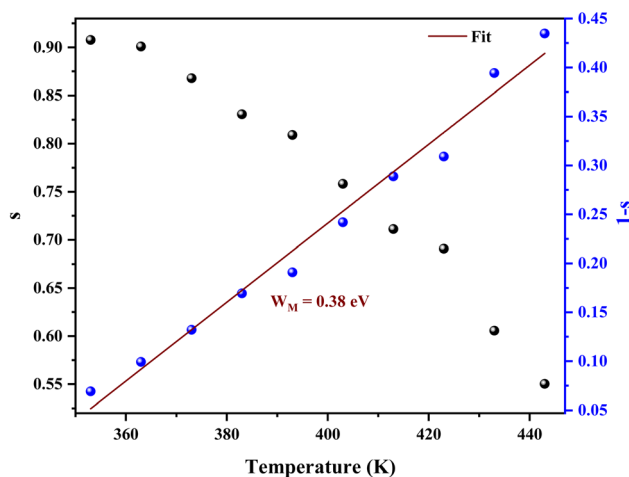
In the CBH model, the charge carriers can move from one location to another by performing a hopping over a potential barrier.[39] The frequency exponent s is represented by following equation:

$$s = 1 - \frac{6k_BT}{W_H + k_BT \ln(\omega\tau_0)} \tag{7}$$

where τ_0 is a characteristic relaxation time $\tau_0 = 10^{-13}$. s and W_H represents the energy needed to move an electron from one location to another one. For the large values of W_H/k_BT is considered, eqn (7) reduces to eqn (8):[40]

$$s = 1 - \frac{6k_BT}{W_H} \tag{8}$$

The average value of the barrier energy W_H *average* was calculated as 0.31 eV by the slope of the line given in Fig. 7. This value is approximately a quarter of the activation energies $\left(\frac{E_a}{4}\right)$ which indicates that the single polaron hopping is the dominating conduction mechanism in $[C_{12}H_{17}N_2]_2ZnBr_4$.[41]

In this formalism, the alternating conductivity ac is given by:[42-44]

$$\sigma_{ac} = \frac{\pi^3 NN_P\varepsilon\varepsilon_0\omega R_\omega^6}{24} \tag{9}$$

where NN_P is proportional to the square of the concentration of states, ε is the dielectric constant of the material and R_ω is the hopping distance for conduction and is given by the relation:

$$R_\omega = \frac{e^2}{\pi\varepsilon_0\varepsilon\left[W_M - k_BT \ln\left(\frac{1}{\omega\tau_0}\right)\right]} \tag{10}$$

NN_P is given by: $NN_P = N_T^2$ (for bipolaron hopping), where N_T is the number of states density. $NN_P = N_T^2 e^{(-U_{eff}/2k_BT)}$ (for single polaron hopping).

The temperature dependence of the ac conductivity for $[C_{12}H_{17}N_2]_2ZnBr_4$ at selected frequencies is reported in Fig. 11.
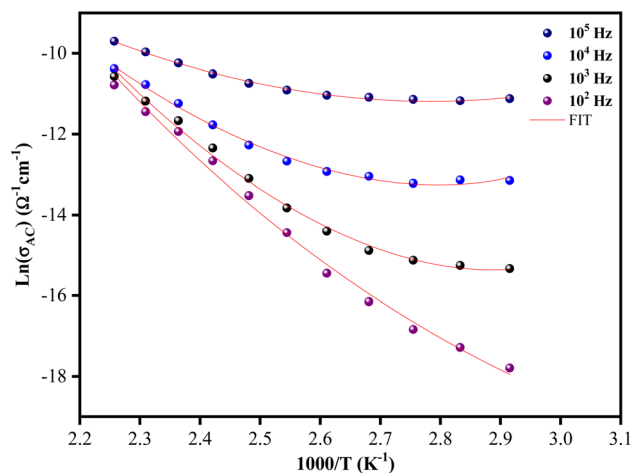

Fig. 10 Temperature dependence of the frequency exponent s and 1 s.

Fig. 11 Evolution of the $\ln(\sigma_{ac})$ *versus* $1000/T$ for the $[C_{12}H_{17}N_2]_2ZnBr_4$ compound.

Table 3 *ac* conductivity parameters used for CBH model fitting for the $[C_{12}H_{17}N_2]_2ZnBr_4$ hybrid material at various frequencies

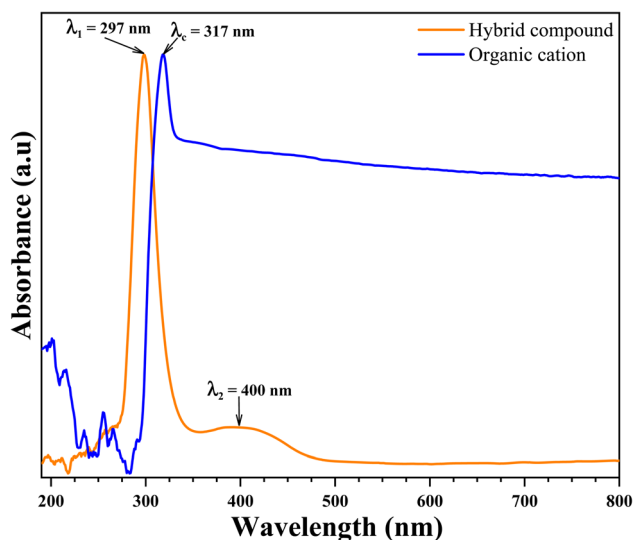| F (Hz)	N_{EF} (eV^{-1} m^{-1})	U_{eff}
10^2	6.8018×10^{13}	-0.08364
10^3	4.4729×10^{14}	-0.08933
10^4	5.3397×10^{15}	-0.0692
10^5	1.1309×10^{16}	-0.04252

Fig. 12 UV-visible absorption spectra of organic cation (blue line) and organic-inorganic hybrid compound (orange line).

Clearly this plots shows that the theoretical calculations fitted by eqn (9) are good with the experimental data. The calculated fitting parameters are listed in Table 3. It can be noted that the

values of the density of states $N(E_F)$ as a function of frequency are reasonable for localized states.[45] Due to the strong electron–phonon interaction, the effective Hubbard intrasite correlation energy U_{eff} is found to be negative.[46]

3.4. Optical properties

3.4.1. UV-visible absorption spectra analysis. UV radiation is therefore an effective tool for the identification and characterization of the structure and absorption of the materials. The absence of absorption bands in the visible region of the grown compound attests to the suitability of the grown materials for photonic and optical applications.[47] The UV-visible absorption spectra of organic cation and cluster study of the spin-coated film was recorded in a range of 200–800 nm (Fig. 12).

As can be seen Fig. 12, the absorption spectrum of organic cation shows one strong distinguished peak centered at $\lambda_c = 317$ nm. This strong absorption peak in the UV region have been attributed to $\pi \rightarrow \pi^*$ transitions in the organic cation ring. This peak has been shifted to the strong distinguished peak centered at $\lambda_1 = 297$ nm appeared in the absorption spectrum of hybrid compound. This shift caused by the new environment (inorganic anion) characterized by the charge transferred from organic cation the inorganic anion. Another medium band centered at $\lambda_2 = 400$ nm is also showed in the absorption spectrum of hybrid compound in visible region. This absorption band have been attributed to metal charge transferred in inorganic anion from metal atom (Zn) to halogen atom (Br).

3.4.2. Band gap analysis. The determination of the optical bandgap E_g was based on the Tauc formula. Since the band gap energy (E_g) controls the optical and electrical properties of materials, it is essential to know and discuss this quantity. The study of the electronic structure and the type of transition of the
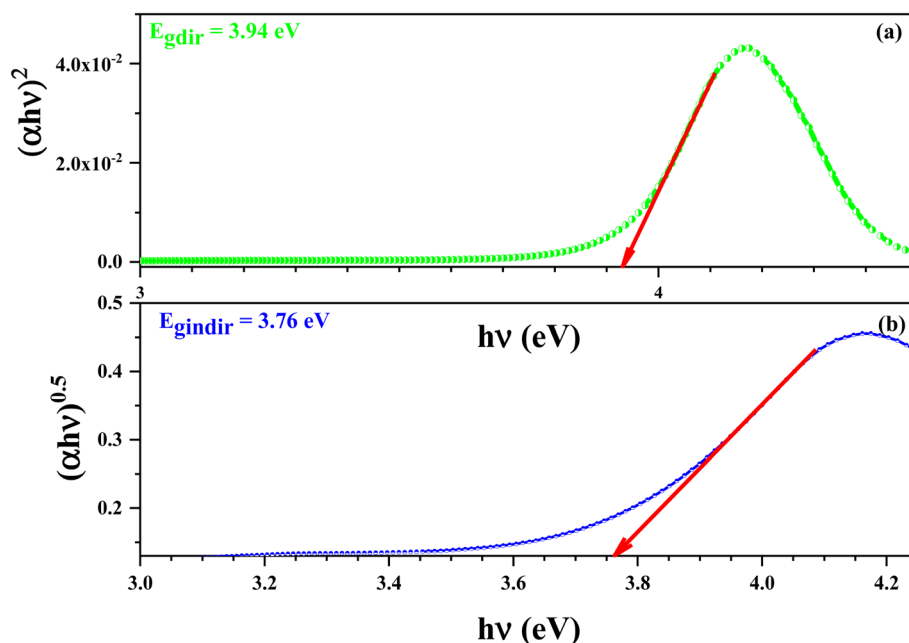

Fig. 13 Variations of $(\alpha h\nu)^2$ (a) and $(\alpha h\nu)^{0.5}$ (b) *versus* $h\nu$ for the $[C_{12}H_{17}N_2]_2ZnBr_4$ compound.

electrons shows us the dependence of the coefficient of optical absorption with the energy of the photons. Using the absorption data, the optical absorption coefficient "α" can be deduced by applying the Beer–Lambert's law:[48]

$$\alpha = \frac{2.3036}{d}\ln\left(\frac{1}{T}\right) = \frac{2.3036}{d}A \tag{11}$$

where, A is the absorbance and d is the thickness of the thin layer.

The absorption coefficient is given by the following Pankove's relation:[49]

$$\alpha h\nu = B\left(h\nu - E_g\right)^{\frac{1}{p}} \tag{12}$$

The coefficient $p = 2$ for allowed direct transitions and $p = 0.5$ for indirect allowed transitions. B is the probability parameter for the transition and E_g the optical bandgap energy.

The E_g value corresponding to direct band gap transitions can be calculated *via* the $(\alpha h\nu)^2$ *versus* $h\nu$, using the formula:

$$(\alpha h\nu)^2 = B(h\nu - E_g) \tag{13}$$

The E_g value corresponding to indirect band gap transitions can be considered *via* the $(\alpha h\nu)^{0.5}$ *versus* $h\nu$, using the formula:

$$(\alpha h\nu)^{0.5} = B(h\nu - E_g) \tag{14}$$

Fig. 13 demonstrate the variation of $(\alpha h\nu)^2$ (a) and $(\alpha h\nu)^{0.5}$ (b) *versus* $h\nu$ of this compound. The values of E_{gd} and E_{gind} were estimated from the intersection of the extrapolated linear part of the $(\alpha h\nu)^2$ and $(\alpha h\nu)^{0.5}$ curves with energy axis.

The values of E_{gd} and E_{gind} were estimated from the intersection of the extrapolated linear part of the $(\alpha h\nu)^2$ and $(\alpha h\nu)^{0.5}$ curves with energy axis. The optical absorption measurement near the fundamental absorption edge is a standard method for estimation of the band gap energy. The direct band gap of the 3.94 eV results in an energy gap of 3.76 eV.

4. Conclusion

In this work, a new $[C_{12}H_{17}N_2]_2ZnBr_4$ sample, with a centrosymmetric $P2_1/n$ space group, was prepared and its optical, electrical and *ac* conductivity are investigated as a function of temperature and frequency. The asymmetric unit is constituted by one tetabromozincate $[ZnBr_4]^{2-}$ anion and two protonated $[C_{12}H_{17}N_2]^+$ cations.

The energy of the optical gap was found to be approximately 3.94 eV for a direct transition and 3.76 eV for an indirect one. This leads us to conclude that the $[C_{12}H_{17}N_2]_2ZnBr_4$ compound is a good candidate for the application of semiconductors.

The Nyquist plots were satisfactorily fitted with the one-cell circuit model R/C/CPE, with the exception of adding a CPE element in series from the temperature of phase transition. The temperature dependency of Z' with an inverse variation suggests a semiconducting behavior. The *ac* conductivity, over the studied temperature and frequency range, is described by Jonscher's power law. The thermal behavior of the extracted

exponent s confirmed that the CBH model is the appropriate model for this compound.

Conflicts of interest

The authors declare that they have no known competing financial interests or personal relationships that could have appeared to influence the work reported in this paper.

References

1 K. E. Lee, N. Morad, T. T. Teng and B. T. Poh, *Chem. Eng. Sci.*, 2012, **203**, 370.
2 F. Garnier, *Chem. Phys.*, 1998, **227**, 253.
3 A. Gagor, M. Wojtas, A. Pietraszko and R. Jakubas, *Acta Crystallogr., Sect. B: Struct. Sci.*, 2008, **64**, 558.
4 A. Oueslati and M. Gargouri, *J. Alloys Compd.*, 2018, **739**, 1089.
5 H. Zhang, X. Wang, K. Zhang and B. K. Teo, *Coord. Chem. Rev.*, 1999, **183**(1), 157.
6 M. Ben Bechir, K. Karoui, M. Tabellout, K. Guidara and A. Ben Rhaiem, *J. Alloys Compd.*, 2014, **588**(5), 551.
7 S. Karoui, S. Kamoun and A. Jouini, *J. Solid State Chem.*, 2013, **197**, 60.
8 B. Saparov and D. B. Mitzi, *Chem. Rev.*, 2016, **116**, 4558.
9 H. Zhang, X. Wang, K. Zhang and B. K. Teo, *Coord. Chem. Rev.*, 1999, **183**, 157.
10 L. Li, M. M. Turnbull, C. P. Landee, J. Jornet, M. Deumal, J. J. Novoa and J. L. Wikaira, *Inorg. Chem.*, 2007, **46**, 11255.
11 S. Wang, D. B. Mitzi, C. A. Field and A. Guloy, *J. Am. Chem. Soc.*, 1995, **117**, 5297.
12 D. B. Mitzi, K. Liang and S. Wang, *Inorg. Chem.*, 1998, **37**, 321.
13 N. Chihaoui, B. Hamdi and R. Zouari, *J. Mol. Struct.*, 2017, 114.
14 I. Chaabane, F. Hlel and K. Guidara, *PMC Phys. B*, 2008, **1**, 1.
15 R. H. Blessing, *Acta Crystallogr., Sect. A: Found. Crystallogr.*, 1995, **51**, 33.
16 G. M. Sheldrick, *SHELXS-97: Program for Crystal Structure Solution*, University of Göttingen: Göttingen, Germany, 1997.
17 G. M. Sheldrick, *SHELXL-97: Program for Crystal Structure Refinement*, University of Göttingen: Göttingen, Germany, 1997.
18 L. J. Farrugia, *J. Appl. Crystallogr.*, 1997, **30**, 565.
19 K. Brandenburg, *Diamond Version 2.0 Impact GbR*, Bonn, Germany, 1998.
20 A. R. Lim, *RSC Adv.*, 2022, **12**, 28720.
21 A. Srinivasa Rao, E. Sunil Babu, K. C. Kumara Swamy and S. K. Das, *Polyhedron*, 2010, **29**, 1706.
22 I. Chaabane, F. Hlel and K. Guidara, *J. Alloys Compd.*, 2008, **461**, 495.
23 N. Kumar, A. Shukla, C. Behera and R. N. P. Choudhary, *J. Alloys Compd.*, 2016, **688**, 858.
24 J. R. Macdonald, *Impedance Spectroscopy*. John Wiley and Sons, New York, 1987.
25 K. Omri, R. Lahouli and L. El Mir, *Results Phys.*, 2019, **12**, 2141.

26 Y. Pu, Z. Dong, P. Zhang, Y. Wu, J. Zhao and Y. Luo, *J. Alloys Compd.*, 2016, **672**, 64.

27 P. Nayak, T. Badapanda, A. K. Singh and S. Panigrahi, *RSC Adv.*, 2017, **7**, 16319.

28 R. Pattanayak, S. Panigrahi, T. Dash, R. Muduli and D. Behera, *Phys. B*, 2015, **474**, 57.

29 D. Johnson, *ZPlot, ZView Electrochemical Impedance Software*, Version 2.3b, Scribner Associates Inc., North Carolina, 2000.

30 B. Behera, P. Nayak and R. N. P. Choudhary, *J. Mater. Sci.: Mater. Electron.*, 2008, **19**, 1005.

31 A. Omri, M. Bejar, E. Dhahri, M. Es-Souni, M. Valente, M. Graça and L. Costa, *J. Alloys Compd.*, 2012, **536**, 173.

32 M. M. Costa, G. F. M. Pires Jr, A. J. Terezo, M. P. F. Graca and A. S. B. Sombra, *J. Appl. Phys.*, 2011, **110**, 034107.

33 M. Hamdi, A. Oueslati, I. Chaabane and F. Hlel, *International Scholarly Research Network ISRN Condensed Matter Physics*, 2012, vol. 1, p. 750497.

34 M. Amine Fersi, I. Chaabane and M. Gargouri, *Phys. E*, 2016, **83**, 306.

35 A. Oueslati, *Ionics*, 2016, **10**, 1878.

36 E. Barsoukov and J. Ross Macdonald, *Impedance Spectroscopy Theory, Experiment, and Applications*, Wiley Interscience, 2005, p. 14.

37 A. K. Pradhan, S. Saha and T. K. Nath, *Appl. Phys. A*, 2017, **123**, 715.

38 I. G. Austin and N. F. Mott, *Adv. Phys.*, 1969, **18**, 41.

39 A. Oueslati, *Ionics*, 2017, **23**, 857.

40 A. A. A. Darwish, E. F. M. El-Zaidia, M. M. El-Nahass, T. A. Hanafy and A. A. Al-Zubaidi, *J. Alloys Compds*, 2014, **589**, 393.

41 G. A. Khan and C. A. Hogarth, *J. Mater. Sci.*, 1991, **26**, 17.

42 M. Jebli, C. Rayssi, J. Dhahri and K. Khirouni, *Appl. Phys. A: Mater. Sci. Process.*, 2020, **126**, 108.

43 A. Zolanvari, N. Goyal and S. K. Tripathi, *Pramana*, 2004, **63**, 617.

44 A. Oueslati and M. Gargouri, *J. Alloys Compd.*, 2018, **739**, 1089.

45 M. Ben Bechir, K. Karoui, M. Tabellout, K. Guidara and A. Ben Rhaiem, *J. Appl. Phys.*, 2014, **115**, 203712.

46 S. R. Elliott, *Adv. Phys.*, 1987, **36**, 135.

47 M. Abid Derbel, S. Nasr, H. Naïli and W. Rekik, *Inorg. Chem. Commun.*, 2022, **142**(6), 109654.

48 J. Wang, X. Deng, F. Zhang, D. Chen and W. Ding, *Nanoscale Res. Lett.*, 2014, **9**, 117.

49 M. Arakha, M. Saleem, C. Mallick Bairagi and S. Jha, *Sci. Rep.*, 2015, **5**, 1.